Measurements in the thick axisymmetric turbulent boundary layer near the tail of a body of revolution

Patel, V. C.

Nakayama, A.

Damian, R.

(Citation)
Journal of Fluid Mechanics,63(2):345-367

(Issue Date)
1974-04

(Resource Type)
journal article

(Version)
Version of Record

(URL)
https://hdl.handle.net/20.500.14094/90001184

J. Fluid Mech. (1974), *vol.* 63, *part* 2, *pp.* 345–367
Printed in Great Britain

Measurements in the thick axisymmetric turbulent boundary layer near the tail of a body of revolution

By V. C. PATEL, A. NAKAYAMA AND R. DAMIAN

Institute of Hydraulic Research, University of Iowa, Iowa City, Iowa 52242

(Received 14 March 1973)

Detailed measurements of pressure distributions, mean velocity profiles and Reynolds stresses were made in the thick axisymmetric turbulent boundary layer near the tail of a body of revolution. The results indicate a number of important differences between the behaviour of a thick and a thin boundary layer. The thick boundary layer is characterized by significant variations in static pressure across it and an abnormally low level of turbulence. The static-pressure variation is associated with a strong interaction between the boundary layer and the potential flow outside it, while the changes in the turbulence structure appear to be a consequence of the transverse surface curvature. In order to predict the behaviour of the flow in the tail region of a body of revolution it is not therefore possible to use conventional thin-boundary-layer calculation procedures.

1. Introduction

A number of previous studies have shown that, when the thickness of the boundary layer on a body of revolution becomes of the same order as the local radius of the body, the influence of transverse (or lateral) curvature, which is usually neglected in thin-boundary-layer theory, becomes appreciable. Such a situation arises in the case of the boundary layer developing on a long slender cylinder placed axially in a stream. This particular configuration has been examined experimentally and theoretically in some detail in previous investigations. In his recent paper Cebeci (1970) has reviewed the previous studies of both laminar and turbulent boundary layers, and also presented the results of his own calculations using finite-difference techniques. For laminar flow the situation appears to be quite satisfactory in so far as Cebeci's numerical results cover a wide range of conditions and also show substantial agreement with the results of other, not so extensive, analytical studies. In the case of the turbulent boundary layer Cebeci employed an eddy-viscosity model with the additional assumption that this model is not directly affected by transverse curvature. Thus, the influence of curvature is taken into account only in the mean-flow momentum and continuity equations. While the results of these calculations show a plausible effect of transverse curvature, and also agree with the experimental results of

Richmond (1957) and Yasuhara (1959), the assumption that the same eddy-viscosity model applies to both thin and thick boundary layers remains to be verified directly since it implies that the turbulent motion itself is not explicitly influenced by transverse curvature. In order to demonstrate the validity of such an assumption it is of course necessary to make detailed turbulence measurements in thick axisymmetric boundary layers. Such measurements have not been reported so far. From the recent study of Patel (1973*a*) it appears that the use of a universal mixing-length or eddy-viscosity model adequately describes the velocity distribution in the wall region of a thick axisymmetric boundary layer. More experimental data are, however, needed to elucidate the turbulent motion in the outer region.

The cylinder problem cited above is ideally suited for studying the influence of transverse curvature on the development of the boundary layer since the absence of pressure gradients in this case enables one to isolate the curvature effect. In many practical situations, however, significant transverse curvature effects occur in conjunction with streamwise pressure gradients, and possibly with longitudinal surface curvature. Well-known examples of this type of flow are the boundary layers in the mid-section of conical and annular diffusers. Another, equally important, case is the flow in the tail region of a body of revolution. In this case the boundary layer over the forward part of the body is thin and can be treated by conventional techniques, but if the body is sufficiently long and slender, the boundary layer in the tail region will grow to a thickness which is comparable with, or even much larger than, the local radius of the body. The present study deals with this latter case. It will be obvious that here we have a case in which both transverse curvature and pressure gradients may dominate the flow. As we shall see later, this flow exhibits several other features of interest; amongst these being a strong interaction between the boundary layer and the potential flow outside it.

This paper describes mean-flow and turbulence measurements in the thick axisymmetric boundary layer on a body of revolution. A parallel theoretical study was undertaken to develop methods for calculating such a thick boundary layer and also to investigate the possibilities of calculating, simultaneously, the potential and boundary-layer flows, allowing the two to interact. The results of these studies will be published separately.

In the literature there are several publications which report measurements on boundary layers in conical diffusers and on bodies of revolution but none of these was made with a view to studying the interaction phenomenon just mentioned. Moreover, there is little information concerning the turbulence in a thick axisymmetric boundary layer. In the case of a body of revolution, the interaction is important since the pressure distribution on the surface is modified considerably by the boundary layer even when the flow does not separate anywhere. The pressure recovery at the tail (or the pressure variation through the boundary layer at the tail) is obviously needed to obtain better estimates of the total drag experienced by the body. The present experiments were designed specifically to study these aspects of the flow.

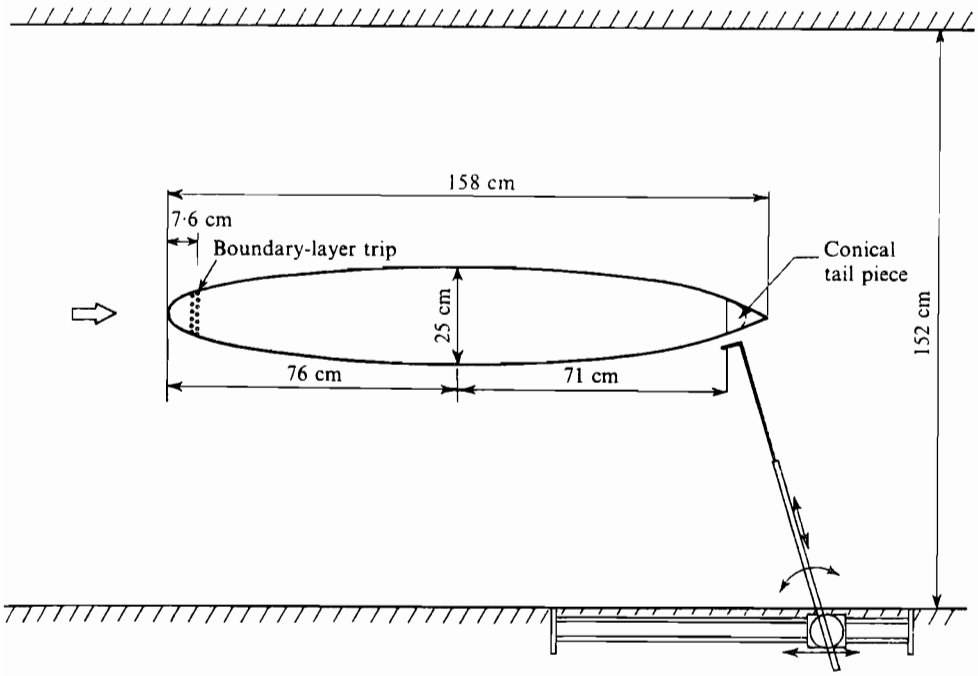

FIGURE 1. Model and traversing mechanism.

2. Experimental arrangement and instruments

2.1. *Wind tunnel*

The experiments were conducted in the largest closed-circuit wind tunnel of the Iowa Institute of Hydraulic Research. The working section of the tunnel is 7·3 m long with a cross-section in the form of a 1·5 m octagon provided by throating a 3·7 m square approach section. Although the maximum speed attainable in the tunnel is of the order of 27 m/s all the measurements reported here were made at a nominal speed of 12 m/s in order to minimize the influence of tunnel vibration.

2.2. *Model, mountings and alignment*

A six-to-one prolate spheroid, 1·5 m long and 25 cm in maximum diameter, used previously by Chevray (1968) to study axisymmetric wakes and by Satija (1971) to make preliminary investigations of axisymmetric boundary layers, was used in the present experiments. Two rows of cylindrical lucite beads, 0·635 cm long, were attached with a spacing of 0·635 cm at a distance of 7·6 cm from the nose to ensure early transition of the boundary layer. In order to avoid separation ahead of the tail, Satija modified the original spheroid used by Chevray by truncating it at a section 5 cm from the tail and glueing on a conical tail piece such that the slope of the surface remained continuous at the junction. With this modification the overall length of the model became 158 cm. The model is shown schematically in figure 1.

The model was mounted in the wind tunnel by means of eight 1 mm diameter

steel wires in tension, four at each end of the model. Each wire was provided with a screw-coupling such that its length could be easily adjusted and the model located at any desired position.

In order to obtain axial symmetry of the boundary layer the geometric axis of the model was first aligned with the centre-line of the tunnel. Three identical Pitot tubes, 6.35 mm in diameter, were then placed in contact with the surface at intervals of 120° around the body at a section about 6·35 cm from the tail. Small adjustments were then made in the lengths of the supporting wires until the total pressures recorded by the three tubes became equal. This procedure was repeated by placing three similar tubes at about the mid-section of the model. Finally, six Pitot tubes were used, three at each of the two sections, the tubes downstream being offset by 60° relative to those upstream. Only minor adjustments were required in this final stage to obtain agreement between the readings of the three tubes at each section. Since the readings of the Pitot tubes may be regarded as a measure of the wall shear stress, and consequently of the velocity distribution in the wall region, this procedure ensured axial symmetry of the flow.

As an additional check on the axial symmetry, the axial components of mean and fluctuating velocities were measured by means of a hot-wire anemometer in the wake of the body 7·6 cm downstream from the tail. Although the measurements were made in only one plane across the wake, the distributions of mean velocity and the root-mean-square values of the fluctuating velocity were found to be closely symmetrical about the geometric axis of the model. From these measurements it was concluded that the boundary layer on the model was axially symmetric to a sufficient degree of accuracy.

2.3. *Traversing mechanism*

The essential features of the traversing mechanism used in the experiments are shown in figure 1. The mechanism consisted of a rigid rod with three degrees of freedom in the horizontal plane passing through the axis of the model: transverse motion along the length of the rod, transverse motion along a slide situated outside the tunnel and rotation about a pivot on this slide. The mechanism was thus capable of traversing measuring probes, such as Pitot tubes and hot-wire probes, mounted on the end of the rod by suitable brackets, in the direction normal to the model surface at a number of discrete streamwise locations on the model. The length of the slide was such that the furthest upstream point on the model which could be investigated was about 66 % of the model length from the nose. For the purpose of the present study this was considered quite adequate. At the other end, measurements could be made right up to the tail of the model. The main rod of the traversing mechanism was provided with a screw drive, a scale and a vernier so that the normal distance of the probes from the model surface could be adjusted and measured from outside the tunnel with a resolution of 0·3 mm. The rod entered the tunnel through a narrow slit cut out of the tunnel wall. The portion of the slit not occupied by the rod was sealed by a rubber sheet to prevent any leakage of air from the tunnel.

The traversing rod had to be made rigid enough to prevent it from vibrating

in the wind. In order to minimize the interference between the traversing mechanism and the flow being measured the probes were attached such that the distance between the probe tip and the traversing rod was as large as possible.

2.4. *Measuring instruments*

All total (Pitot) and static pressures were measured using probes of standard design, made from hypodermic tubing of outside diameters 1·27 mm and 1·65 mm respectively, in conjunction with micromanometers capable of resolving pressure differences of the order of 0·025 mm alcohol. The air temperature and pressure in the tunnel were measured immediately downstream of the contraction. These, together with the barometric pressure and dry- and wet-bulb temperatures in the laboratory, were used to find the density and viscosity of the air as well as to correct the manometer readings in the manner suggested by Naudascher (1964).

Mean velocities and the Reynolds stresses within the boundary layer on the model were measured by means of single- and X-wire probes using the two-channel, constant-temperature 'Old Gold Model, Type 4-2H Hot-Wire Anemometer' and 'Type 2 Mean-Product Computer', designed and manufactured by the Iowa Institute of Hydraulic Research. These instruments are built with all solid-state electronic components and equipped with a linearizing circuit for each hot-wire channel and an analog-to-frequency converter. Other features of the design and principles of operation of this anemometer system have been described by Glover (1972). The single-wire and X-wire probes used in the measurement of mean and fluctuating velocity components were all made from copper-plated tungsten wires of nominal diameter 0·00287 mm and resistance 8440 Ω/m.

Preliminary experiments conducted at the beginning of the present study, as well as those made earlier by Satija, indicated an unrealistically low level of turbulence in the boundary layer on the spheroidal model. After a considerable amount of experimentation, the origin of this anomaly was traced to an inadequate frequency response of the hot-wire anemometer. Once this had been discovered, modifications were made in the amplifier circuits to improve the frequency response and at the same time to cut down the noise level. The necessary modifications were relatively minor. In order to ensure that the modified system performed adequately, a number of tests were conducted in fully developed turbulent pipe flow. A copper pipe 5 cm in diameter and 10 m long was constructed for this purpose. Measurements with Pitot tubes, and single-wire and X-wire probes, were then made a few inches upstream of the pipe exit, and the results compared with those of Laufer (1954). Satisfactory agreement was obtained with the data of Laufer as regards the distributions across the pipe of the mean velocity, the Reynolds shear stress and the turbulent normal stresses (i.e. the mean-square values of the three components of the velocity fluctuation).

In addition to providing a check on the performance of the hot-wire anemometer, the pipe experiments also served to highlight the problems, such as drift in the calibration curves and the necessity of having identical calibration curves

for both wires in X-wire operation, associated with the use of the instruments. These tests also suggested the techniques to be followed in subsequent experiments in order to obtain reliable and consistent data.

3. Some observations from preliminary experiments

Exploratory measurements in the boundary layer on the spheroidal model were first made by traversing the total-head and static-pressure tubes separately across the boundary layer at a number of streamwise stations ranging from about 66 % of the model length to the tail. Both tubes were oriented parallel to the model surface. These measurements indicated, amongst other things, that the boundary layer remained attached right up to the tail and that large variations in static pressure occurred across the boundary layer over the last 10 % of the model length. This variation in static pressure was accompanied by a dramatic increase in the thickness of the boundary layer.

Before describing the detailed measurements which were made later on, it is convenient to discuss briefly the consequences of these early observations. The rapid thickening of the boundary layer and the large variations in the static pressure in the direction normal to the body surface of course indicated that the mean-flow streamlines within the boundary layer did not remain closely parallel to the surface. Alternatively, the component of velocity normal to the wall could no longer be assumed to be an order of magnitude smaller than the component parallel to the wall, as is the case in thin boundary layers. A number of important conclusions pertaining to the measuring techniques follow immediately.

(i) Since the direction of the mean-flow streamlines changes continuously across the boundary layer, a simple static-pressure probe mounted parallel to the body surface cannot be relied upon to give an accurate measure of the local static pressure, especially at large distances from the surface. If such a probe is to be used with any success its orientation must be changed continuously to coincide with the local streamline direction, which is not known *a priori*.

(ii) A properly designed total-head tube can be made insensitive to yaw angles up to 30° so that it can be used in the present situation without incurring appreciable errors.

(iii) Owing to the difficulty of measuring static pressure mentioned above, the Pitot-static combination cannot be used to measure the velocity distribution across the boundary layer.

(iv) In order to measure the velocity profiles in the tail region it is therefore necessary to use hot-wire techniques. A single hot-wire probe traversed normal to the body surface will, however, give the distribution of the resultant velocity through the boundary layer but not the angle which the velocity vector makes with the surface of the body.

(v) The variation in static pressure through the boundary layer can in principle be determined by taking the difference between the total head measured by a Pitot tube and the dynamic pressure recorded by means of a single wire. As we shall see later, this procedure is not altogether satisfactory, although consistent results can be obtained when due care is taken.

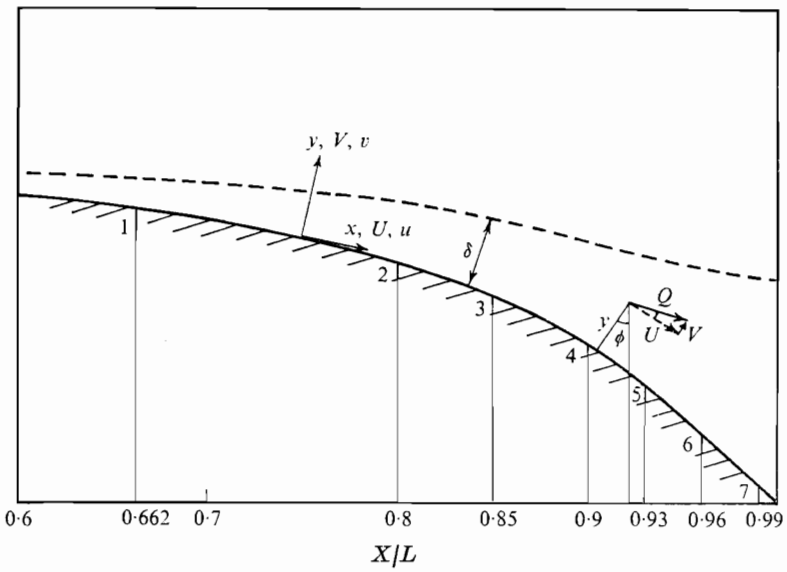

FIGURE 2. Measuring stations and notation.

(vi) To specify the velocity field in the tail region of the body completely, it is necessary to measure the components of mean velocity along and normal to the body surface. This can best be accomplished by traversing a X-wire probe in the direction normal to the surface.

(vii) The use of X-wire probes to measure mean velocities has the additional advantage that the Reynolds normal and shear stresses can also be measured at the same time.

The above conclusions contributed in large measure to the final procedures adopted for making the measurements reported below. Traverses of total-head and static-pressure tubes, and single-wire and X-wire probes, were made at seven streamwise stations on the model, namely $X/L = 0{\cdot}662$, $0{\cdot}80$, $0{\cdot}85$, $0{\cdot}90$, $0{\cdot}93$, $0{\cdot}96$ and $0{\cdot}99$, where X denotes the distance from the nose of the model measured along the axis and L the overall length ($= 157{\cdot}8$ cm) of the model. All measurements were made at a nominal unit Reynolds number of $8{\cdot}0 \times 10^5\,\mathrm{m}^{-1}$.

The relative positions of the seven measuring stations and the notation adopted for the presentation of data are shown in figure 2. The complete model is described by the radius distribution

$$\frac{r_0}{L} = \begin{cases} \frac{1}{6}\left\{\frac{X}{L}\,0{\cdot}9655 - \frac{X}{L}\right\}^{\frac{1}{2}}, & 0 < \frac{X}{L} < 0{\cdot}9333, \\ 0{\cdot}4333\left(1 - \frac{X}{L}\right), & 0{\cdot}9333 < \frac{X}{L} < 1{\cdot}000. \end{cases}$$

The angle between the tangent to the surface and the axis of the model is ϕ. x and y are curvilinear co-ordinates measured along and normal to the surface, respectively. If r is the distance of a point from the model axis, it follows that

$$r = r_0 + y\cos\phi.$$

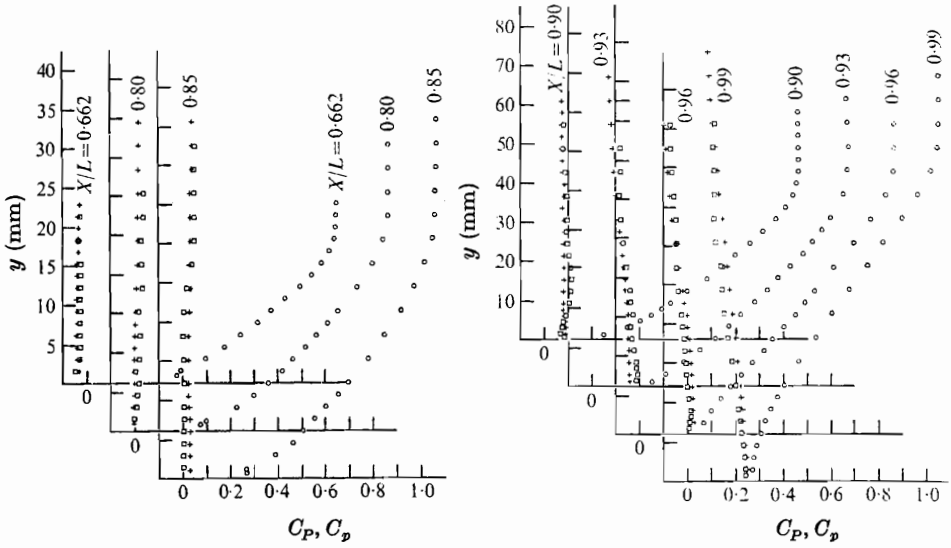

FIGURE 3. Variation of total- and static-pressure coefficients.
○, C_P; +, C_p, static tube; □, C_p, single wire and total pressure.

The components of mean velocity along x and y are U and V, respectively. The resultant velocity at any point is denoted by Q, so that $Q = (U^2 + V^2)^{\frac{1}{2}}$. The velocity fluctuations will be denoted by lower-case letters. In addition to these, we have the total pressure P, the static pressure p, density ρ and kinematic viscosity ν. Subscripts w and δ will be used to signify values at the wall ($y = 0$) and at the edge of the boundary layer ($y = \delta$), respectively.

4. Mean-flow measurements

The total-head (Pitot) tube described earlier was first tested for insensitivity to yaw and then traversed through the boundary layer, keeping the tube parallel to the body surface, at each of the seven streamwise measuring stations. The total pressure was measured relative to the static pressure p_{ref} in the tunnel just downstream from the contraction and made dimensionless by division by the tunnel dynamic pressure $\frac{1}{2}\rho U_{\text{ref}}^2$, which was held constant in all tests. The measured variations of the total-pressure coefficient $C_P = (P - p_{\text{ref}})/\frac{1}{2}\rho U_{\text{ref}}^2$ are shown in figure 3. Since C_P becomes independent of y outside the boundary layer, these measurements were used to estimate the boundary-layer thickness δ. The variation of δ and the ratio δ/r_0 with streamwise distance is shown in figure 4.

Similar measurements were then made using the static-pressure tube and the data were rendered dimensionless using the same reference conditions as before. The variations of the static-pressure coefficient $C_p = (p - p_{\text{ref}})/\frac{1}{2}\rho U_{\text{ref}}^2$ are also shown in figure 3. As indicated in the last section, these static-pressure measurements may be suspect in the outer regions of the boundary layer over the last 10 % of the length of the model owing to the yaw sensitivity of the probe. They are, however, included here for comparison with results obtained by an alter-

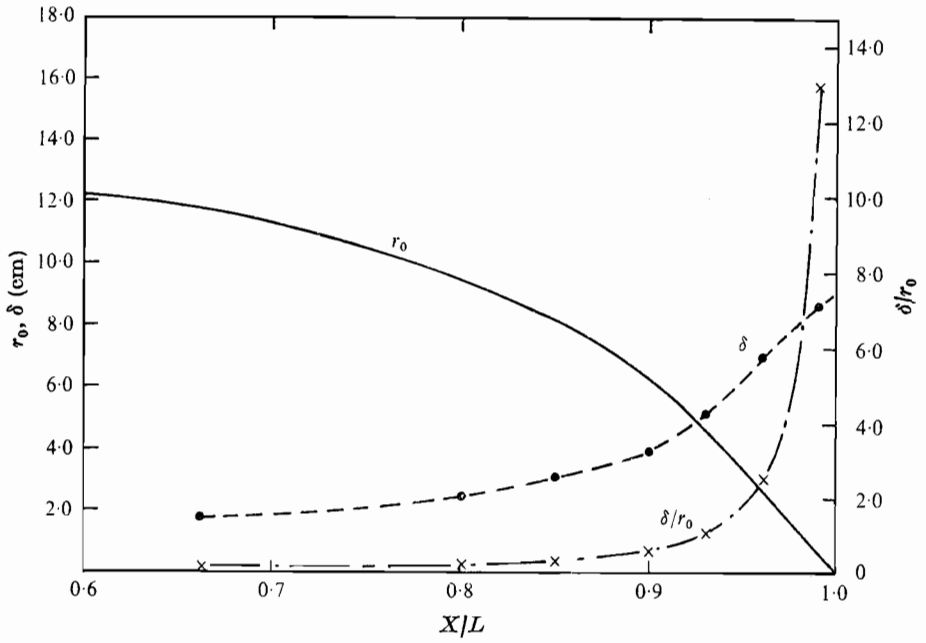

FIGURE 4. Variation of boundary-layer thickness and local radius of the body.

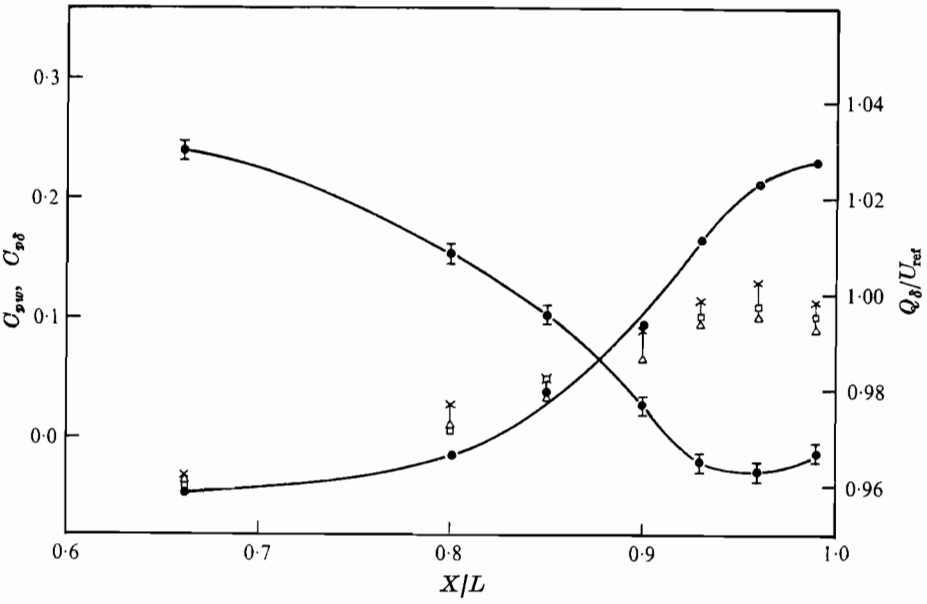

FIGURE 5. Variation of wall static pressure and pressure and velocity at the edge of the boundary layer. $\overline{\bullet}$, Q_δ/U_{ref}; ●, C_{pw}; ×, $C_{p\delta}$ (total pressure and single wire); □, $C_{p\delta}$ (static tube); △, $\overline{C}_{p\delta}$ (Bernoulli equation and Q_δ).

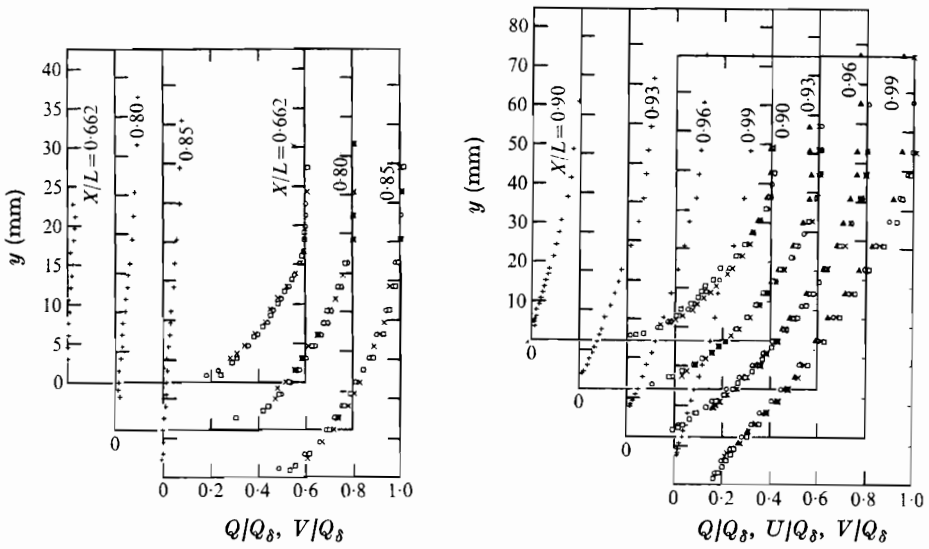

FIGURE 6. Mean-velocity profiles. Q/Q_δ: ○, Pitot static; ×, X-wire; □, single wire. ▲, U/Q_δ, X-wire; +, V/Q_δ, X-wire.

native method. Since the measurements close to the wall are not in doubt even up to the tail (the flow being locally parallel to the wall), the streamwise variation of the static pressure C_{pw} on the model surface was determined by extrapolating the measurements to the wall. A plot of C_{pw} versus X/L is made in figure 5, from which it will be seen that the pressure gradient on the wall is adverse all the way from the first measuring station to the tail. The variation of the static pressure $C_{p\delta}$ at the edge of the boundary layer indicated by the static probe, aligned with the model surface, is also shown in figure 5. Although the accuracy of the results for X/L greater than 0·93 may be questionable, the figure indicates clearly the large static-pressure variations across the boundary layer near the tail of the model. The other results shown in figure 5 are described later on.

From the total- and static-pressure distributions described above, it was possible to calculate the profiles of total velocity, i.e. Q/Q_δ. These are shown in figure 6.

A single hot-wire probe was then traversed through the boundary layer at each of the seven streamwise stations. The wire was held normal to the flow and parallel to the model surface. In these, as well as other hot-wire measurements, care was taken to ensure that the drift of the wire calibration curve was small. Those runs in which the calibration drifted by unduly large amounts were repeated. The profiles of total velocity measured by means of the single wire are compared with those obtained from the Pitot-static measurements in figure 6. The values of Q_δ, the velocity at the edge of the boundary layer, recorded by the single-wire probe are shown in figure 5. Also shown in this figure is the pressure variation $C_{p\delta}$ along the edge of the boundary layer implied by the measured values of Q_δ and the constancy of total pressure.

As mentioned in the last section, the total-pressure profiles measured by the

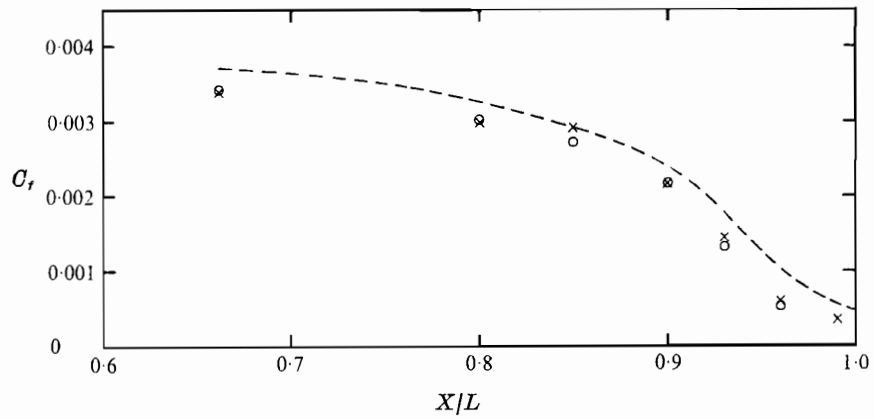

FIGURE 7. Variation of the skin-friction coefficient. ○, Preston tube; ×, Clauser plots; – – –, Thompson, $C_f = C_f(\bar{H}, \bar{R}_\theta)$.

Pitot tube (shown in figure 3) and the total-velocity profiles measured by the single-wire probe were used to infer the static-pressure distributions through the boundary layer. The results of this exercise were not altogether satisfactory, primarily owing to the fact that the static pressure came out as a small difference between two relatively large quantities, neither of which could be measured with the required accuracy. Some consistency was, however, obtained by smoothing the data before taking the differences. The resulting distributions of static pressure are compared with those measured by means of the static-pressure tube in figures 3 and 5.

In order to determine the components of mean velocity U and V along and normal to the model surface, respectively, a X-wire probe was traversed across the boundary layer at each of the seven measuring stations. A probe with the proper geometric and calibration characteristics was built after several trials. The wires were located in the plane normal to the surface and the flow. The results of the X-wire measurements were converted to profiles of U/Q_δ, V/Q_δ and Q/Q_δ. These profiles are also shown in figure 6.

Finally, a Preston tube of outside diameter 3·11 mm was used, in conjunction with the calibration curve of Patel (1965), to determine the wall shear stress τ_w. A plot of the skin-friction coefficient $C_f = \tau_w/\frac{1}{2}\rho Q_\delta^2$ is made in figure 7.

5. Analysis of the mean-flow measurements

5.1. *Boundary-layer growth*

From the variation of the boundary-layer thickness shown in figure 4 it is clear that for about the first 85 % of the body length the boundary layer may be regarded as thin in so far as δ is much smaller than r_0, the local radius of the body. Over the last 15 % of the body length, however, thin-boundary-layer theory will cease to apply and transverse curvature effects are expected to play a dominant role in the behaviour of the flow.

5.2. *Static-pressure distribution*

Although, as indicated earlier, the static-pressure distributions obtained by the two methods may be suspect as far as accuracy in the tail region of the body is concerned, the results shown in figures 3 and 5 confirm the observation made above. The static pressure remains substantially constant through the boundary layer right up to $X/L = 0{\cdot}90$. From figure 5 we see that up to this point the pressure at the edge of the boundary layer is somewhat larger than that at the wall. In addition to the well-known influence of the normal Reynolds stress $\overline{v^2}$, this increase in pressure with distance from the wall may partly be attributed to the convex curvature of the mean-flow streamlines associated with the convex longitudinal curvature of the body surface.

The decrease in static pressure from the wall towards the edge of the boundary layer in the tail region of the body ($X/L > 0{\cdot}90$), on the other hand, appears to be a consequence of the concave curvature of the mean-flow streamlines associated primarily with the rapid thickening of the boundary layer. The change from the thin- to the thick-boundary-layer behaviour seems to take place in the region of the $X/L = 0{\cdot}90$ station, where δ/r_0 is approximately 0·62.

The rapid increase in the thickness of the boundary layer near the tail of the body may of course be regarded as a direct consequence of the ever-increasing influence of transverse curvature, but the large variation in static pressure across the boundary layer associated with this thickening suggests that there is a strong interaction between the boundary-layer flow and the potential flow outside it. Owing to the presence of the thick boundary layer, potential-flow theories can no longer be expected to predict the pressure field in the tail region correctly. At the same time, it is unlikely that usual thin-boundary-layer theory, which assumes constant static pressure in the direction normal to the surface, can adequately predict the boundary-layer behaviour even when the experimentally determined wall-pressure distribution is prescribed. Thus, it appears that any rational theory describing the flow in the tail region of a body of revolution with a thick boundary layer must attempt to solve for the potential flow and the boundary-layer flow simultaneously.

5.3. *Velocity distributions*

Referring to figure 6, it will be seen that the profiles of the total velocity Q/Q_δ measured by the three different methods, namely with Pitot and static tubes, single hot-wire probes and X-wire probes, are in reasonable agreement at all streamwise stations. Although we had expected to observe systematic differences between the Pitot-static and the hot-wire results in the outer parts of the boundary layer near the tail of the body, owing to the yaw sensitivity of the static-pressure tube, figure 6 indicates that any differences which may exist are swamped by the general scatter of the data. Detailed calculations indicated that the expected differences were too small to be distinguished from experimental scatter since the errors incurred in the measurement of static pressure were themselves much smaller than the dynamic pressures from which the total velocities were

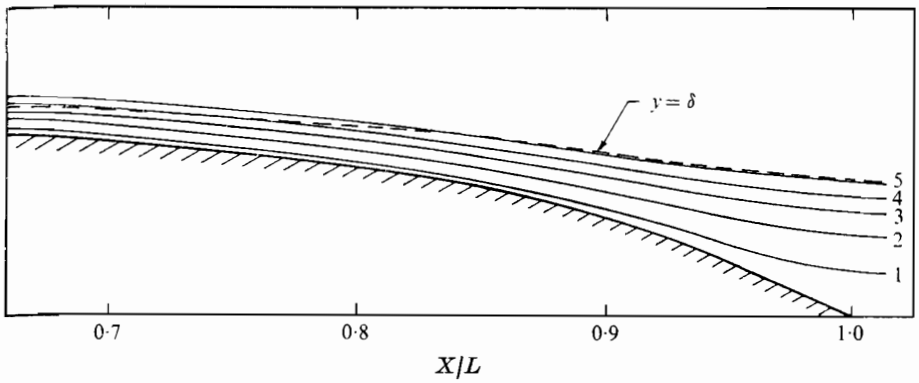

FIGURE 8. Mean-flow streamlines computed from velocity profiles. Values of ψ/L^2U_{ref}: 1, 0·000052; 2, 0·00026; 3, 0·00052; 4, 0·00078; 5, 0·00104.

calculated. The agreement between the results of three different instruments in a complex flow situation such as this was considered very encouraging.

The profiles of the longitudinal and normal components of mean velocity measured by means of the X-wire probe clearly show the difference between the thin and the thick boundary layer. Up to $X/L = 0{\cdot}90$ the normal component of velocity is seen to be small compared with the longitudinal component, as required in thin-boundary-layer theory. By $X/L = 0{\cdot}99$, however, the normal component of velocity is almost 32 % of the longitudinal component at the edge of the boundary layer. Apart from indicating the breakdown of the usual thin-boundary-layer assumptions in the tail region, these results confirm the observation made earlier regarding the rapid divergence of the mean-flow streamlines in planes normal to the surface. Indeed, the angle between the surface and the streamline passing through $y = \delta$ at $X/L = 0{\cdot}99$ is $\tan^{-1} 0{\cdot}32 = 18{\cdot}0°$. Since the angle between the tangent to the body surface at this point and the body axis is $\cos^{-1} 0{\cdot}92 = 23°$, this indicates that the flow near the edge of the boundary layer is more nearly parallel to the axis than the body surface.

The general shape of the velocity profile at the last measuring station shows that the flow there is close to separation. The profile at the most upstream station, $X/L = 0{\cdot}662$, was found to conform well with the two-parameter velocity-profile family of Thompson (1965), indicating that the boundary layer there has essentially the same characteristics as one developing on a plane two-dimensional surface.

5.4. *The mean-flow streamlines*

The longitudinal component of velocity measured by means of the X-wire probe, namely U, was used to compute the distribution of the stream function ψ at each streamwise measuring station, using the definition

$$\psi(y) = \int_0^y Ur\,dy = \int_0^y U(r_0 + y\cos\phi)\,dy.$$

Figure 8 shows the mean-flow streamlines within the boundary layer determined from these distributions of ψ. It will be seen that the streamlines are convex and

nearly parallel to the surface in the region $0{\cdot}662 < X/L < 0{\cdot}90$, where the boundary layer is thin, and concave and divergent over the last 10% of the body length. Figure 8 thus verifies directly the observations made in § 5.2 simply on the basis of static-pressure variations. The angles between the streamlines and the body surface obtained from figure 8 were found to be in good agreement with those deduced from the direct measurements of the normal and longitudinal components of velocity. This may be regarded as a check on the axial symmetry of the boundary layer.

Figure 8 shows yet another interesting feature of the thick boundary layer near the tail. From the near coincidence of the edge of the boundary layer with a mean-flow streamline it may be concluded that the entrainment of free-stream fluid into the thick boundary layer is small.

5.5. *Integral parameters from velocity profiles*

The thickness of the boundary layer at each measuring station was determined from the total-pressure profiles measured by means of the Pitot tube. Thus, δ was defined as the normal distance from the wall where the total pressure became 0·99 times the constant value in the free stream. This definition appears to be the most appropriate one here for two reasons. First, it gives a unique value of δ even when the static pressure, and therefore the velocity, vary with distance from the wall outside the boundary layer. Second, it reduces to the usual definition of δ, as being the distance where the local velocity is 0·995 times the free-stream velocity, when the boundary layer is thin and the static pressure substantially constant across it.

For an axisymmetric boundary layer there appear to be a number of different ways of defining integral parameters such as the displacement and momentum thicknesses.

Perhaps the most meaningful definitions are the *physical definitions*:

$$\int_{r_0}^{r_0+\delta_1^* \cos\phi} 2\pi r\rho U_p \, dr = \int_{r_0}^{r_0+\delta \cos\phi} 2\pi r\rho (U_p - U)\, dr \tag{1}$$

and

$$\int_{r_0}^{r_0+\delta_2^* \cos\phi} 2\pi r\rho U_p^2 \, dr = \int_{r_0}^{r_0+\delta \cos\phi} 2\pi r\rho U (U_p - U)\, dr, \tag{2}$$

where U_p is the velocity distribution which would occur if the flow were potential right up to the wall, δ_1^* is the physical mass-flux deficit thickness, δ_2^* is the momentum-flux deficit thickness and, as noted before, $r = r_0 + y\cos\phi$. The shape factor of the velocity profile and the momentum-thickness Reynolds number of the boundary layer may then be defined as

$$H^* = \delta_1^*/\delta_2^*, \quad R_\theta^* = Q_\delta \delta_2^*/\nu, \tag{3}$$

respectively. The displacement thickness defined in this manner gives the physical displacement of the external flow streamlines due to the presence of the boundary layer, while the momentum thickness is closely related to the drag experienced by the body. The evaluation of these thicknesses from measured velocity profiles is, however, made difficult by the fact that nothing is known about the variation of the velocity distribution U_p in the hypothetical potential

flow over the distance occupied by the boundary layer. If it is assumed that U_p remains constant, and equal to U_δ, over this distance, then (1) and (2) simplify to yield

$$\delta_1^*\left(1+\frac{1}{2}\frac{\delta_1^*}{r_0}\cos\phi\right) = \int_0^\delta \left(1-\frac{U}{U_\delta}\right)\frac{r}{r_0}\,dy \tag{4}$$

and

$$\delta_2^*\left(1+\frac{1}{2}\frac{\delta_2^*}{r_0}\cos\phi\right) = \int_0^\delta \frac{U}{U_\delta}\left(1-\frac{U}{U_\delta}\right)\frac{r}{r_0}\,dy. \tag{5}$$

If the axisymmetric boundary-layer equations are integrated across the layer in the usual manner to obtain the momentum-integral equation, it is found that the integrals on the right-hand sides of (4) and (5) arise quite naturally. In almost all previous studies of axisymmetric boundary layers, therefore, the displacement and momentum thicknesses have been defined simply as

$$\delta_1 = \int_0^\delta \left(1-\frac{U}{U_\delta}\right)\frac{r}{r_0}\,dy \tag{6}$$

and

$$\delta_2 = \int_0^\delta \frac{U}{U_\delta}\left(1-\frac{U}{U_\delta}\right)\frac{r}{r_0}\,dy, \tag{7}$$

so that

$$H = \delta_1/\delta_2, \quad R_\theta = Q_\delta\delta_2/\nu. \tag{8}$$

We shall refer to these as the *usual axisymmetric definitions*. A major advantage of using these is that they enable the momentum-integral equation for axisymmetric flow to be written in a form that is simple and very similar to that for plane-surface boundary layers. As we shall see later, however, these definitions lead to some anomalies when the boundary layer is thick in comparison with the local radius of the body. From the expressions given above it will be clear that the usual axisymmetric definitions are related to the physical definitions (using $U_p \simeq U_\delta$) by the formulae

$$\delta_1 = \delta_1^*(1+\tfrac{1}{2}(\delta_1^*/r_0)\cos\phi) \tag{9}$$

and

$$\delta_2 = \delta_2^*(1+\tfrac{1}{2}(\delta_2^*/r_0)\cos\phi). \tag{10}$$

Finally, if one is interested only in describing the shape of the velocity profiles, without regard to the geometry of the surface, one can determine the thicknesses using the usual definitions:

$$\bar{\delta}_1 = \int_0^\delta \left(1-\frac{U}{U_\delta}\right)dy, \tag{11}$$

$$\bar{\delta}_2 = \int_0^\delta \frac{U}{U_\delta}\left(1-\frac{U}{U_\delta}\right)dy, \tag{12}$$

$$\bar{H} = \bar{\delta}_1/\bar{\delta}_2, \quad \bar{R}_\theta = Q_\delta\bar{\delta}_2/\nu. \tag{13}$$

We shall refer to these as the *planar definitions* for obvious reasons.

It will be clear that the physical definitions as well as the usual axisymmetric definitions reduce to the planar definitions given above when the boundary layer is thin, i.e. when $\delta \ll r_0$. For thick boundary layers, however, the numerical values of the various integral parameters calculated using the three definitions are considerably different.

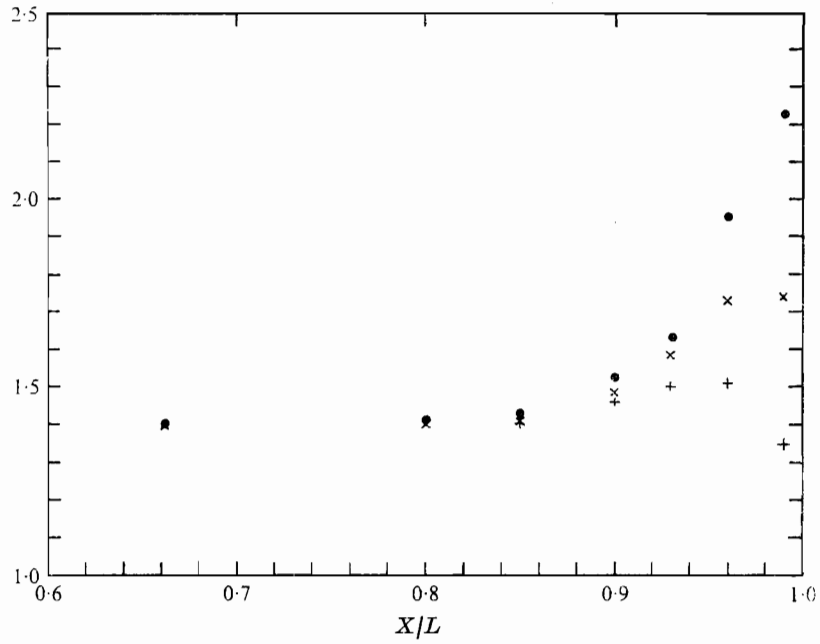

FIGURE 9. Variation of shape factors using different definitions.
●, $\bar{H}$; ×, H; +, H^*.

For the present experiments the integral parameters were calculated at each streamwise station using all three definitions given above. In the calculation of the thicknesses given by the physical definitions, however, the assumption $U_p \simeq U_\delta$ was not used. Instead, use was made of the distribution of U_p implied by the constancy of total pressure and the observed variation of static pressure, since this would appear to represent the true variation of U_p more realistically. The difference between the values calculated in this manner and those obtained using (9) and (10) was found to be of the order of a few per cent. Since the profiles of U/U_δ and Q/Q_δ were not substantially different at the first three measuring stations, namely $X/L = 0{\cdot}662$, 0·80 and 0·85, it was decided to use for these the values of Q/Q_δ indicated by the Pitot and static tubes so as to minimize the influence of the scatter in the hot-wire data. For the last four measuring stations, however, the profiles of U/U_δ recorded by the X-wire probe were used. The results of these calculations are presented in figures 9 and 10.

From figure 9 we see that the nearness to separation at the tail of the body is indicated only by the large value of the shape parameter $\bar{H}$, which is based solely on the shape of the velocity profile. The other two definitions do not convey this important information. Examination of figure 10 indicates the large differences in the numerical values of the momentum thickness resulting from the three alternative definitions. It is interesting to note that, when the boundary layer is much thicker than the local radius of the body (e.g. at $X/L = 0{\cdot}99$), the usual axisymmetric definitions lead to the rather incongruous situation where the momentum and displacement thicknesses become larger than the physical

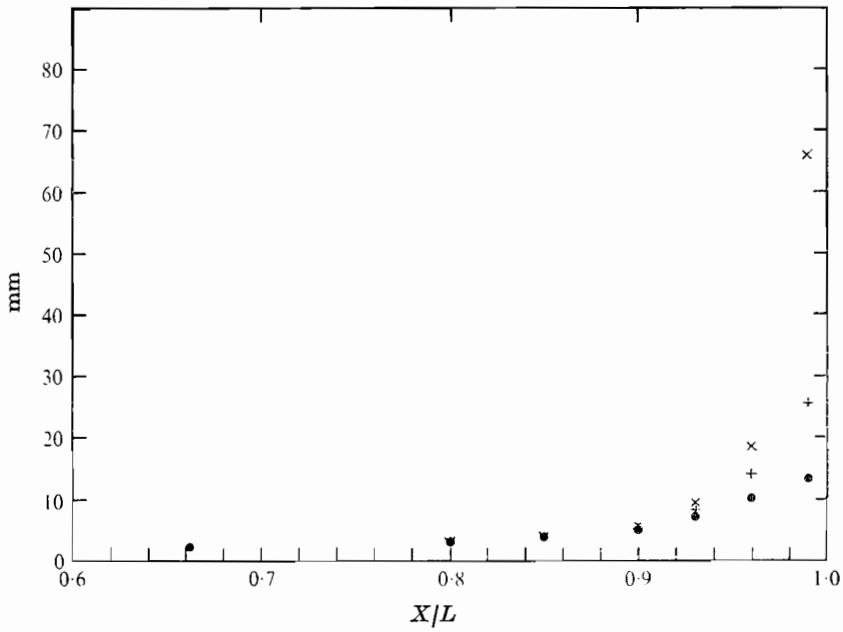

FIGURE 10. Variation of momentum thickness using different definitions. ●, $\bar{\delta}_2$; ×, δ_2; +, δ_2^*.

thickness of the boundary layer. (This is of course due to the ever-increasing factor $1/r_0$ appearing in the definitions.) Considerable care may therefore be required in choosing the most meaningful and appropriate definitions of the integral parameters when attempts are made to extend some of the more successful integral calculation methods to treat thick axisymmetric boundary layers.

5.6. *Wall shear stress*

The values of the wall shear stress, measured directly by means of Preston tubes, are compared in figure 7 with those obtained by applying the method of Clauser (1956) to the profiles of longitudinal velocity U/U_δ. Also shown in the figure is the variation of C_f obtained from the formula of Thompson (1965) using the measured values of the planar parameters $\bar{H}$ and $\bar{R}_\theta$. The disagreement between this formula and the Preston-tube and Clauser-plot results appears to imply that the well-known two-parameter representation of velocity profiles, upon which the skin-friction formula of Thompson is based, may not adequately describe the velocity profiles in thick axisymmetric boundary layers. This observation was indeed confirmed by detailed comparisons of the measured profiles with Thompson's profile family. It may be remarked here that the use of integral parameters other than those obtained from the planar definitions will not lead to improved correlation between experiment and skin-friction and velocity profile relations commonly used in thin-boundary-layer analysis.

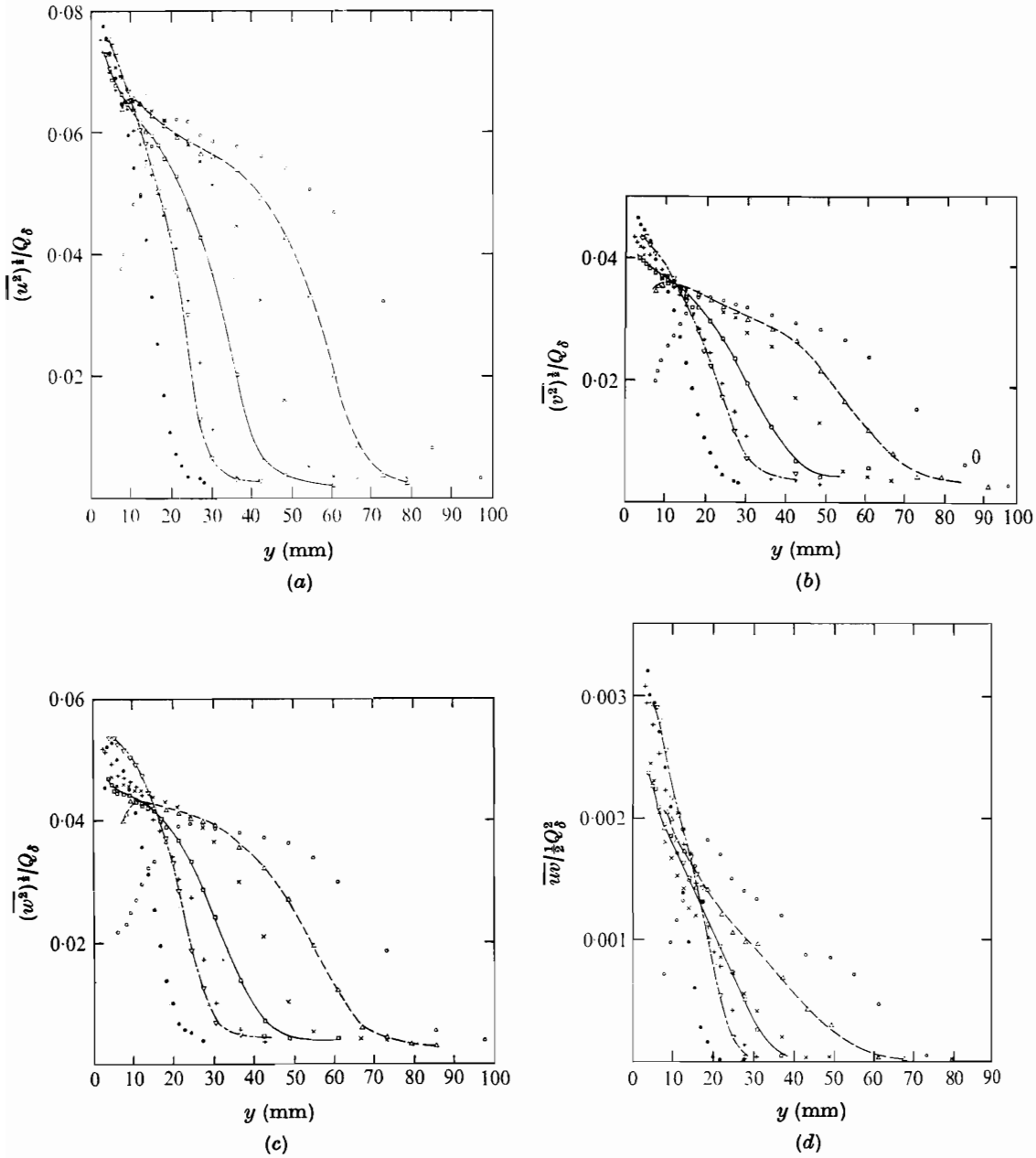

FIGURE 11. (*a*) Longitudinal velocity fluctuations $\overline{(u^2)^{\frac{1}{2}}}/Q_\delta$, (*b*) normal velocity fluctuations $\overline{(v^2)^{\frac{1}{2}}}/Q_\delta$, (*c*) transverse velocity fluctuations $\overline{(w^2)^{\frac{1}{2}}}/Q_\delta$ and (*d*) variation of Reynolds shear stress $\overline{uv}/\frac{1}{2}Q_\delta^2$.

	●	▽	+	□	×	△	○
X/L	0·662	0·80	0·85	0·90	0·93	0·96	0·99

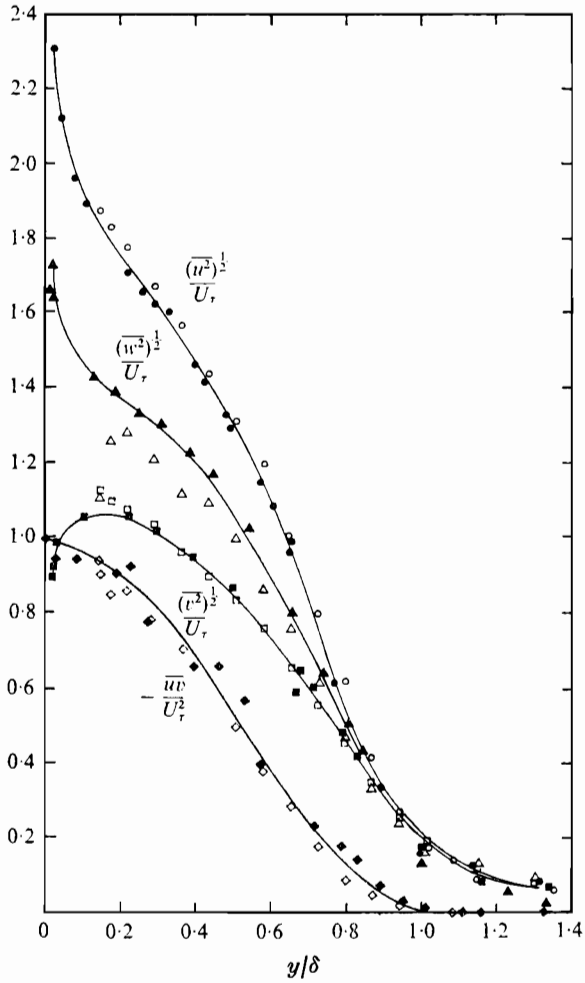

FIGURE 12. Comparison between the turbulence measurements at $X/L = 0{\cdot}662$ (open symbols) and the data of Klebanoff (solid symbols).

6. Measurements of the Reynolds stresses

In the present experiments the Reynolds stresses $\overline{uw}$ and $\overline{vw}$ were assumed to be identically zero on account of the axial symmetry. The remaining components of the Reynolds stress tensor, namely $\overline{u^2}$, $\overline{v^2}$, $\overline{w^2}$ and $\overline{uv}$, were measured by means of X-wire probes. The results were made dimensionless using the velocity at the edge of the boundary layer and are shown in figures 11 (*a*)–(*d*).

The well-known turbulence measurements of Klebanoff (1955) in a flat-plate boundary layer are compared with the present measurements at the most upstream station, $X/L = 0{\cdot}662$, in figure 12. The small disagreement between the two sets of data may be attributed largely to the small adverse pressure gradient which exists at this station and the uncertainties associated with the determination of the boundary-layer thickness. Nevertheless, the trends shown in figure 12

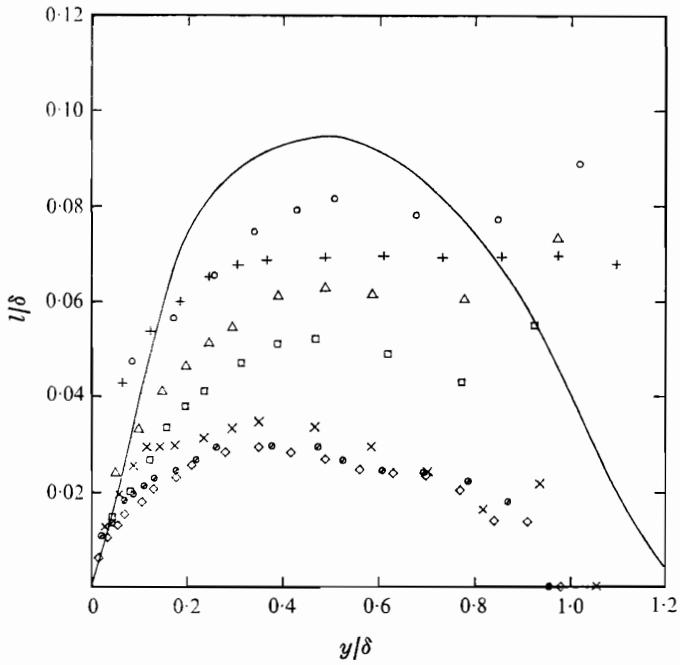

FIGURE 13. Mixing-length profiles. ——, Bradshaw *et al.* (thin boundary layer).

	○	+	△	□	×	◇	◇
X/L	0·662	0·80	0·85	0·90	0·93	0·96	0·99

indicate that the boundary layer at the most upstream measuring station has the properties of a fully developed, thin, turbulent boundary layer.

Perhaps the most striking characteristic of the data shown in figure 11 is the generally low level of turbulence in the thick boundary layer near the tail of the body. In a thin boundary layer that is proceeding towards separation the velocity fluctuations and the shear stresses are much larger than those observed here. From the measurements of shear stress and mean velocities the distributions of mixing length l and eddy kinematic viscosity ϵ were determined using the usual relations

$$-\overline{uv} = l^2(\partial U/\partial y)^2, \quad -\overline{uv} = \epsilon\, \partial U/\partial y. \tag{14}$$

These are shown in figures 13 and 14. It may be remarked here that the variations of mixing length were also found using an axisymmetric definition in the form

$$-\overline{uv} = l_A^2 \left\{\frac{1}{r}\frac{\partial}{\partial y}(Ur)\right\}^2. \tag{15}$$

The values of l_A determined in this manner were found to be substantially lower than those shown in figure 13, especially near the tail. In figure 13 a comparison is made between the experimental distributions of l and the universal distribution used by Bradshaw, Ferriss & Atwell (1967) in the calculation of thin boundary

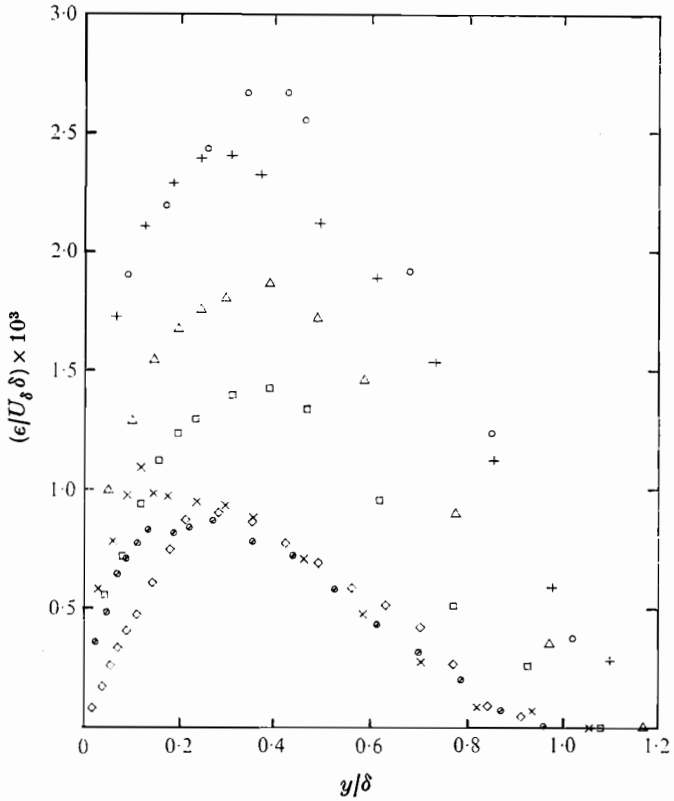

FIGURE 14. Eddy-viscosity profiles. Symbols as in figure 13.

layers. From figures 13 and 14 it is clear that there is a systematic and dramatic decrease in the mixing length and eddy viscosity as the boundary-layer thickness increases in relation to the local radius of the surface.

In recent discussions of energy transport processes in thin boundary layers the mixing length is often associated with a dissipation length on the assumption that the production and dissipation of turbulent kinetic energy are much larger than either diffusion or convection in the wall region, and nearly balance each other. If such an interpretation is accepted for the present case, the reduction in mixing length observed here implies that the rate of dissipation in a thick boundary layer is larger than that in a thin boundary layer. This, coupled with the lower rates of production resulting from the reduced Reynolds stresses, would appear to suggest that the near equilibrium between production and dissipation is no longer maintained in the thick boundary layer, and that the increased rate of dissipation must be accompanied by increased rates of convection and diffusion. More detailed turbulence measurements are obviously needed in order to verify these observations.

7. Conclusions

Perhaps the most useful purpose served by the present study is the collection of a complete set of experimental data in a hitherto unexplored situation. This data can form the basis for further theoretical studies on a number of aspects of turbulent boundary-layer behaviour.†

The major conclusions of this study may be summarized as follows.

(i) The turbulent boundary layer on the conical tail of a body of revolution thickens very rapidly. This thickening is accompanied by (*a*) significant variations in static pressure across the boundary layer such that fluid elements further away from the surface experience smaller adverse pressure gradients than those nearer the surface; (*b*) a strong divergence of the mean-flow streamlines in planes normal to the surface, so that the normal velocity component cannot be neglected in comparison with the longitudinal component; and (*c*) a dramatic decrease in the Reynolds stresses, so that empirical laws established for turbulence behaviour in thin boundary layers cannot be used, unmodified, for the prediction of thick boundary layers.

(ii) The static-pressure variation across the boundary layer implies an interaction between the turbulent rotational flow within the boundary layer and the potential flow outside, with the result that neither can be calculated independently of the other.

(iii) In order to calculate the development of the thick boundary layer, it will be necessary to include not only the direct effects of pressure variation but also the indirect effect of transverse curvature on the turbulence as reflected in the decrease in mixing length and eddy viscosity.

(iv) The boundary-layer calculation is made all the more difficult by the fact that potential-flow theory, which ignores the presence of the boundary layer, can no longer be relied upon to predict the pressure field required to calculate the boundary-layer development. The prediction of the flow in the tail region of a body of revolution must therefore be accomplished by an iterative procedure in which potential-flow and boundary-layer calculations are performed simultaneously. Further discussion of the differential and integral equations of thick axisymmetric boundary layers, and the problems associated with their solution, is given in a recent paper by Patel (1973*b*).

The authors wish to thank Professor L. Landweber for introducing them to the problem. The authors also acknowledge the assistance offered by Professor J. R. Glover in the use of hot-wire anemometers, and by Mr Dale Harris, and his workshop staff, in the construction of the experimental apparatus. This report is based upon research conducted under the General Hydromechanics Research Program of the Naval Ship Systems Command, technically administered by the Naval Ship Research and Development Center, under Contract N00014-68-A-0196-0002.

† Tables of all experimental results are available from the authors upon request.

REFERENCES

BRADSHAW, P., FERRISS, D. H. & ATWELL, N. P. 1967 Calculation of boundary layer development using the turbulent energy equation. *J. Fluid Mech.* **28**, 593.

CEBECI, T. 1970 Laminar and turbulent incompressible boundary layers on slender bodies of revolution in axial flow. *J. Basic Engng, Trans. A.S.M.E.* D **92**, 545.

CHEVRAY, R. 1968 The turbulent wake of a body of revolution. *J. Basic Engng, Trans. A.S.M.E.* D **90**, 275.

CLAUSER, F. H. 1956 The turbulent boundary layer. *Adv. in Appl. Mech.* **4**, 1.

GLOVER, J. R. 1972 'Old Gold Model, Type 4-2H Hot-Wire Anemometer' and 'Type 2 Mean-Product Computer'. *Iowa Inst. Hydraul. Res. Rep.* no. 136.

KLEBANOFF, P. S. 1955 Characteristics of turbulence in a boundary layer with zero pressure gradient. *N.A.C.A. Tech. Rep.* no. 1247.

LAUFER, J. 1954 The structure of turbulence in fully developed pipe flow. *N.A.C.A. Tech. Rep.* no. 1174.

NAUDASCHER, E. 1964 Effect of density on air-tunnel measurements. *J. Roy. Aero. Soc.* **68**, 419.

PATEL, V. C. 1965 Calibration of the Preston tube and limitations on its use in pressure gradients. *J. Fluid Mech.* **23**, 185.

PATEL, V. C. 1973*a* A unified view of the law of the wall using mixing-length theory. *Aero. Quart.* **24**, 55.

PATEL, V. C. 1973*b* On the equations of a thick axisymmetric turbulent boundary layer. *Iowa Inst. Hydraul. Res. Rep.* no. 143.

RICHMOND, R. L. 1957 Experimental investigation of thick axially symmetric boundary layers on cylinders at subsonic and hypersonic speeds. Ph.D. thesis, California Institute of Technology, Pasadena.

SATIJA, K. S. 1971 On the thick boundary layer near the tail of a body of revolution. Ph.D. thesis, University of Iowa, Iowa City.

THOMPSON, B. G. J. 1965 A new two-parameter family of mean velocity profiles for incompressible turbulent boundary layers on smooth walls. *Aero. Res. Counc. R. & M.* no. **3463**.

YASUHARA, M. 1959 Experiments of axisymmetric boundary layers along a cylinder in incompressible flow. *Trans. Japan Soc. Aerospace Sci.* **2**, 33.